Journal of Biomechanics 174 (2024) 112269

Contents lists available at ScienceDirect

Journal of Biomechanics

journal homepage: www.elsevier.com/locate/jbiomech

# Quantifying irregular pulsation of intracranial aneurysms using 4D-CTA

Hujin Xie [a,b], Han Yu [a,b], Hao Wu [c], Jiaqiu Wang [a,b,d], Shanglin Wu [a,b], Jianjian Zhang [e], Huilin Zhao [e], Mingyang Yuan [a,b], Jessica Benitez Mendieta [a,b], Haveena Anbananthan [a,b], Craig Winter [f], Chengcheng Zhu [g], Zhiyong Li [a,b,h,*]

[a] School of Mechanical, Medical and Process Engineering, Queensland University of Technology, Brisbane, QLD 4000, Australia
[b] Centre for Biomedical Technologies, Queensland University of Technology, Brisbane, QLD 4000, Australia
[c] School of Biological Science & Medical Engineering, Southeast University, Nanjing 210096, Jiangsu, China
[d] School of Engineering, London South Bank University, London, United Kingdom
[e] Department of Radiology, Ren Ji Hospital, Shanghai Jiao Tong University School of Medicine, 160 Pujian Road, Shanghai, China
[f] The Kenneth G Jamieson Department of Neurosurgery, Royal Brisbane and Women's Hospital, Brisbane, QLD 4006, Australia
[g] Department of Radiology, University of Washington School of Medicine, Seattle, WA, United States
[h] Faculty of Sports Science, Ningbo University, Ningbo 315211, Zhejiang, China

ARTICLE INFO

*Keywords:*
4D-CTA
Intracranial aneurysm
Irregular pulsation
Strain

ABSTRACT

Recent studies have suggested that irregular pulsation of intracranial aneurysm during the cardiac cycle may be potentially associated with aneurysm rupture risk. However, there is a lack of quantification method for irregular pulsations. This study aims to quantify irregular pulsations by the displacement and strain distribution of the intracranial aneurysm surface during the cardiac cycle using four-dimensional CT angiographic image data. Four-dimensional CT angiography was performed in 8 patients. The image data of a cardiac cycle was divided into approximately 20 phases, and irregular pulsations were detected in four intracranial aneurysms by visual observation, and then the displacement and strain of the intracranial aneurysm was quantified using coherent point drift and finite element method. The displacement and strain were compared between aneurysms with irregular and normal pulsations in two different ways (total and stepwise). The stepwise first principal strain was significantly higher in aneurysms with irregular than normal pulsations ($0.20 \pm 0.01$ vs $0.16 \pm 0.02$, $p = 0.033$). It was found that the irregular pulsations in intracranial aneurysms usually occur during the consecutive ascending or descending phase of volume changes during the cardiac cycle. In addition, no statistically significant difference was found in the aneurysm volume changes over the cardiac cycle between the two groups. Our method can successfully quantify the displacement and strain changes in the intracranial aneurysm during the cardiac cycle, which may be proven to be a useful tool to quantify intracranial aneurysm deformability and aid in aneurysm rupture risk assessment.

## 1. Introduction

Intracranial aneurysm (IA) is a vascular lesion that refers to a localized swelling and distension of the blood vessels in the brain. Approximately 2 % to 5 % of the global population is estimated to suffer from IAs (D'Urso et al., 2011; Timmins et al., 2021; Vlak et al., 2011). The rupture of IA can cause serious complications, such as subarachnoid haemorrhage (SAH), which is a dangerous condition that requires prompt medical intervention and carries with it a significant risk of death, long-term injury rates and high costs (Bakker et al., 2023; Hu et al., 2023).

Currently, clinical intervention decisions prioritize patient age, aneurysm size, and location (Greving et al., 2014; Rinkel, 2019; Sforza et al., 2009). To further evaluate the aneurysm rupture risk, some

* Corresponding author at: School of Mechanical, Medical and Process Engineering, Queensland University of Technology, (QUT) 2 George St, Brisbane, QLD 4000, Australia.

*E-mail addresses:* hujin.xie@qut.edu.au (H. Xie), h27.yu@qut.edu.au (H. Yu), 836924359@qq.com (H. Wu), jiaqiu.wang@lsbu.ac.uk (J. Wang), shanglin.wu@hdr.qut.edu.au (S. Wu), zjj-1108@163.com (J. Zhang), huilinzhao2013@163.com (H. Zhao), mingyang.yuan@hdr.qut.edu.au (M. Yuan), j2.benitezmendieta@qut.edu.au (J. Benitez Mendieta), haveenanandhini.anbananthan@hdr.qut.edu.au (H. Anbananthan), Craig.Winter@health.qld.gov.au (C. Winter), zhucheng043@gmail.com (C. Zhu), zhiyong.li@qut.edu.au (Z. Li).

https://doi.org/10.1016/j.jbiomech.2024.112269
Accepted 6 August 2024
Available online 7 August 2024

haemodynamic parameters have been developed by using computational fluid dynamics (CFD) (Can and Du, 2016; Hosseini et al., 2021; Khan et al., 2021; Li et al., 2022; Li et al., 2020), such as the oscillatory shear index (OSI), the pressure loss coefficient (PLc), and the wall shear stress (WSS). In addition, four-dimensional CT angiography (4D-CTA) has also been used to evaluate IAs rupture risk. This imaging method provides a series of images of the aneurysm over time, enabling the visualization of changes in size and shape (Diab et al., 2023). It was used to analyze the relationship between the rate of morphological change during the cardiac cycle and IA rupture risk (Kuroda et al., 2012), and it was found that the rate of change in the height and volume of IA domes during a cardiac cycle was an independent factor associated with aneurysm rupture risk (Wang et al., 2023). Recently, the irregular pulsation observed from 4D-CTA was suggested to be a potential factor for IA rupture risk, as it may indicate a localized weakening of the aneurysm wall (Vanrossomme et al., 2015). Several recent studies have utilized 4D-CTA with electrocardiographic (ECG) gated reconstruction to identify irregular pulsation as a potential indicator of aneurysm instability (Ferrari et al., 2016; Gu et al., 2020). One study reported that the area of irregular pulsation detected by 4D-CTA was consistent with the site of aneurysm rupture based on a small sample of ruptured aneurysms (Hayakawa et al., 2011). Another study that focused on unruptured aneurysms found that irregular pulsation was associated with changes in morphology on follow-up imaging, indicating a higher risk of aneurysm rupture (Hayakawa et al., 2014). One recent study stated the prevalence of irregular pulsation was much higher in the ruptured and symptomatic aneurysms compared with the asymptomatic group, which included 305 patients with 328 aneurysms (37 ruptured, 60 symptomatic, 231 asymptomatic) (Zhang et al., 2023). Therefore, irregular pulsations of IA are considered to be associated with or may indicate, a risk of rupture. However, the identification of irregular pulsations is currently carried out through manual evaluation in previous studies (Zhang et al., 2021; Zhang et al., 2023). It is worth noting that this manual process may cite variations due to subjective factors, and a better and more automatic approach to quantifying irregular pulsations may help clinicians identify irregular pulsations in a more standardized manner. Therefore, quantifying aneurysm surface motion (displacement and strain) is needed (Xie et al., 2024), which can directly show the location of large deformation on the IA surface. To the best of our knowledge, there are no studies in the literature focused on the quantification of IA surface displacement and strain associated with irregular pulsations based on 4D-CTA.

This paper proposed a coherent point drift finite element method (CPD-FEM) for quantifying the IA surface motion using 4D-CTA imaging. This method consists of two main steps: first, tracking the IA's motion during the cardiac cycle using the CPD algorism to obtain the displacement with finite element mesh, followed by strain analysis on the aneurysm surface via the Green-Lagrange strain tensor in FEM. Eight patient-specific IA models are analyzed, and IA's displacement and strain changes during the cardiac cycle are quantified. The study aims to quantify and compare the displacement and strain values between aneurysms with irregular and normal pulsations.

## 2. Materials and methods

### 2.1. Study design and 4D-CTA imaging

This retrospective study included eight patients with IAs who underwent 4D-CTA from January 2018 to July 2021 in Renji Hospital, Shanghai, China. Eight intracranial aneurysms were included in this study, and four aneurysms were found to have irregular pulsation. The presence of irregular pulsation (defined as a temporary focal protuberance occurring in at least three consecutive frames) was decided by two neuroradiologists (JZ and HZ), both with six years of experience in the diagnosis of neurovascular CTA (Zhang et al., 2023). The inclusion and exclusion criteria are provided in the Appendix. The study was approved by the Queensland University of Technology Human Research Ethics Committee (Project Reference ID: 2022–6108-10078), and written informed consent was obtained from all participants.

**Table 1**
Patient information.

| Patient ID | Age | Sex | IA Location | Size (mm) | Irregular pulsation |
|---|---|---|---|---|---|
| 1 | 58 | F | L-ICA | 14 | Yes |
| 2 | 57 | F | R-MCA | 9.1 | Yes |
| 3 | 64 | F | L-MCA | 9.7 | Yes |
| 4 | 73 | M | R-ICA | 4.9 | Yes |
| 5 | 54 | F | L-ICA | 11 | No |
| 6 | 74 | F | R-MCA | 7.4 | No |
| 7 | 73 | F | R-MCA | 10.5 | No |
| 8 | 62 | F | R-MCA | 5.1 | No |

ICA, internal carotid artery; MCA, middle cerebral artery.

For 4D-CTA image acquisition, a 320-detector row CT scanner (Aquilion ONE VISION, Canon Medical System Corporation, Otawara, Japan) was used to scan the cerebral arteries with a prospective ECG-gated scan mode performed within one cardiac cycle, and the spatial resolution of the 4D-CTA data is $0.31 \times 0.31 \times 0.5\ mm^3$, and was performed with the injection of 60 mL intravenous contrast medium at 3–4 mL/s (iomeprol 400 mg/mL, Iomeron; Bracco, Milan, Italy) (Zhang et al., 2023). Segmentation and reconstruction included 20 phases of R-R interval from 0 % to 95 % every 5 % cardiac cycle (20 frames across the cardiac cycle). Table 1 shows the patient details, and the segmentation procedures are provided in the Appendix.

### 2.2. Surface motion tracking

By performing the segmentation procedures in the Appendix, we obtained point cloud data for different phases of the IA during the cardiac cycle. The CPD was used for surface motion tracking to obtain the IA surface displacement (Myronenko and Song, 2010). The CPD algorithm views the alignment of two-point clouds as a probability density estimation. The source cloud matches the Gaussian Mixture Model (GMM) centroids, and the reference cloud matches the fixed data points. The source point cloud, here the first phase data, is moved coherently as a group until the maximum likelihood is achieved, which means that the two data sets are optimally aligned.

The GMM probability function for a point $x$ can be defined as follows

$$p(x) = \sum_{m-1}^{M+1} P(m)p(x|m) \tag{1}$$

Where $M$ $(m = 1, \cdots, M)$ is the point in the GMM which will generate $N$ $(x = 1, \cdots, N)$ new points. We can then re-parameterize the locations of the GMM centroids by a set of parameters $\theta$ and estimate them by maximizing the likelihood as follows

$$E(\theta, \sigma^2) = -\sum_{n-1}^{N} log \sum_{m-1}^{M+1} P(m)p(x_n|m) \tag{2}$$

where $\sigma^2$ is the isotropic covariances. The CPD algorithm allows for a large initial displacement of both point clouds. It does not require initial alignment, nor does the proposed data-matching algorithm require both point clouds to have the same number of data points. The core of this approach is to force the GMM centroids to move coherently as a group, thus preserving their topology. Fig. 1 shows an example (Patient 4) used for intracranial aneurysm surface motion tracking. Fig. 1(a) shows two-point clouds, the fixed-point cloud (green) and the moving-point cloud (purple), and the number of purple and green points are different. Fig. 1 (b) shows the two point clouds after motion tracking by the CPD method, and the purple point cloud was perfectly aligned with the green point cloud.

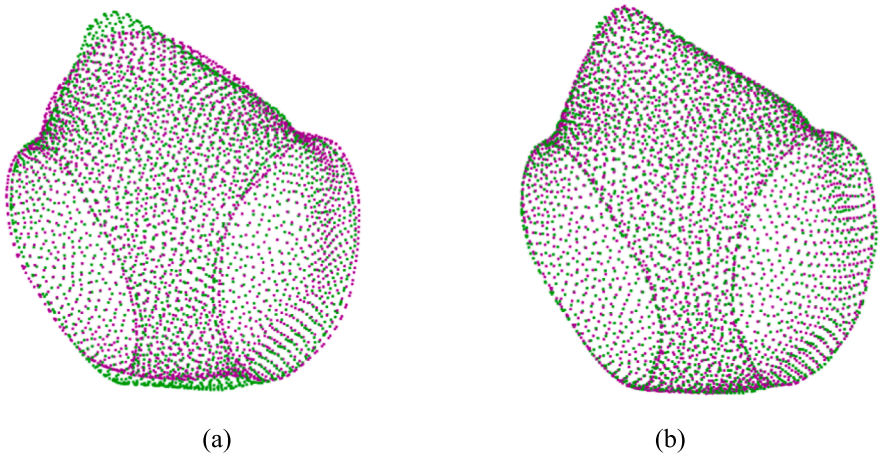


**Fig. 1.** The two-point clouds, the fixed-point cloud (green) and the moving-point cloud (purple): (a) The two-point clouds before motion tracking and (b) The two-point clouds after motion tracking. (For interpretation of the references to colour in this figure legend, the reader is referred to the web version of this article.)

### 2.3. Strain computation

From a mechanical point of view, an intracranial aneurysm can be assumed as a thin-walled nonlinear membrane or shell structure (Lu et al., 2008; Ma et al., 2007). Blood vessels are often considered to have no bending stiffness, primarily due to their nonlinear material properties and lower stiffness at low strain, similar to fabric materials. Additionally, mechanical tests have shown that the wall tissue has negligible bending stiffness (Humphrey and Canham, 2000). Therefore, membrane elements with triangular mesh are used for strain calculation (Ma et al., 2004), and the IAs (Patients 1 to 4) with irregular pulsation were meshed into 10414, 7322, 8196 and 4554 elements, respectively. Due to the complex structure and composition of the aneurysm, the surface deformation of IAs exhibits a complex mechanical behaviour, with the largest deformations usually occurring where irregular pulsation occurs, which is also likely to be where the aneurysm wall is weaker. Therefore, we use the Green-Lagrange strain to address the problem of large deformations of aneurysms, and a reference phase is selected for strain computation based on the criterion that the sum of the spatial distances from all surface points of the phase to the centroid is the smallest.

The Green-Lagrange strain tensor can be defined in matrix form as

$$\boldsymbol{E} = \begin{bmatrix} E_{xx} & E_{xy} & E_{zx} \\ E_{xy} & E_{yy} & E_{yz} \\ E_{zx} & E_{yz} & E_{zz} \end{bmatrix} \tag{3}$$

The principal strain refers to the maximum and minimum strains experienced by a material at a specific point when subjected to deformation. To find the principal strains, we need to solve the eigenvalue

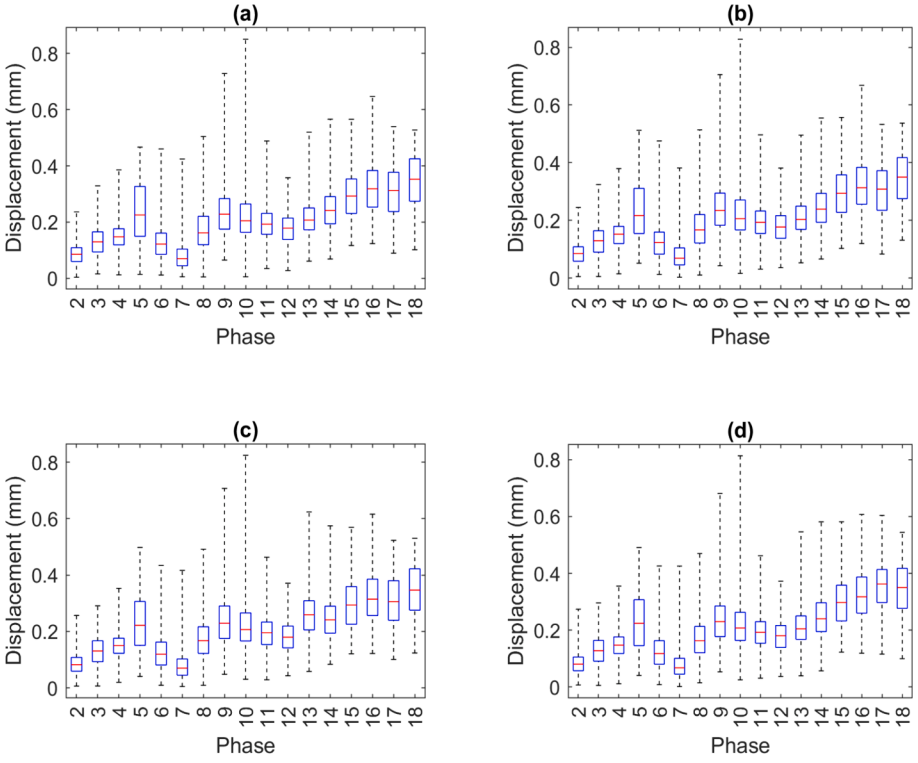


**Fig. 2.** Self-validation results for the relative spatial variation in displacement compared to Phase 1: (a) Phase 5 as reference; (b) Phase 9 as reference; (c) Phase 13 as reference; and (d) Phase 17 as reference.

**Table 2**
Euclidean distance (root mean square error) between the aligned point clouds.

| Patient ID | 1 | 2 | 3 | 4 | 5 | 6 | 7 | 8 |
|---|---|---|---|---|---|---|---|---|
| **Minimum (mm)** | 0.1252 | 0.1116 | 0.1638 | 0.0764 | 0.1130 | 0.1211 | 0.0920 | 0.0729 |
| **Maximum (mm)** | 0.1256 | 0.1151 | 0.1574 | 0.0818 | 0.1332 | 0.1229 | 0.0967 | 0.0776 |

problem for the strain tensor in (3). This involves finding the eigenvalues ($\lambda$) and corresponding eigenvectors ($\phi$) of the strain tensor as follows

$$eig\begin{bmatrix} E_{xx} & E_{xy} & E_{zx} \\ E_{xy} & E_{yy} & E_{yz} \\ E_{zx} & E_{yz} & E_{zz} \end{bmatrix} = \begin{bmatrix} E_1 \\ E_2 \\ E_3 \end{bmatrix} \tag{4}$$

Where the eigenvalues $\lambda_1$, $\lambda_2$, and $\lambda_3$ represent the first principal strain $E_1$, second principal strain $E_2$ and third principal strain $E_3$ respectively. The Von Mises strain has also been considered and calculated as follows

$$E_v = \sqrt{\frac{1}{2}\left[\left(E_{xx}-E_{yy}\right)^2+\left(E_{yy}-E_{zz}\right)^2+\left(E_{zz}-E_{xx}\right)^2+6\left(E_{yz}^2+E_{zx}^2+E_{xy}^2\right)\right]} \tag{5}$$

Furthermore, we also defined a space strain in our strain computation, which is evaluated from three normal strains as follows

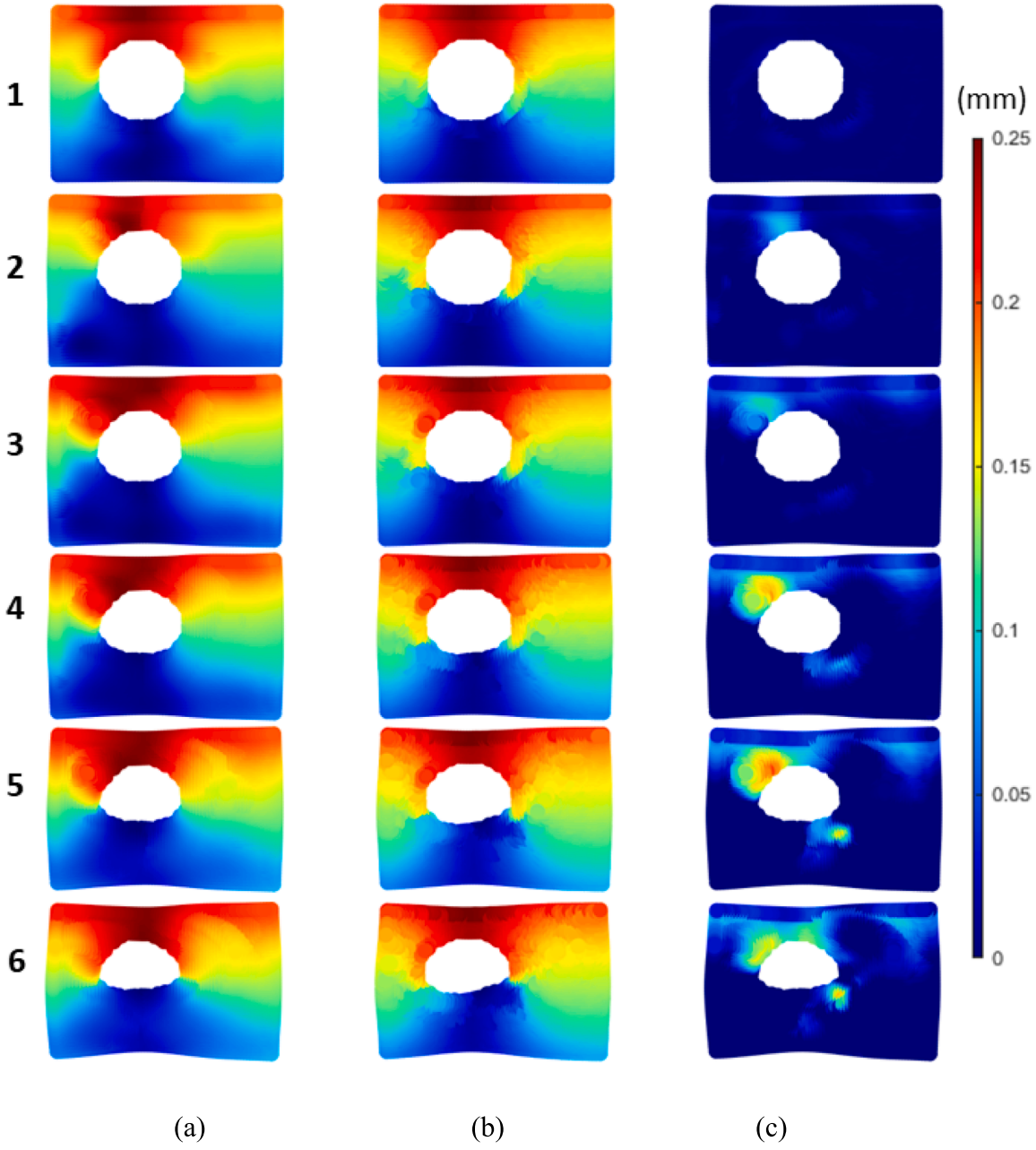


**Fig. 3.** The displacement results from compression stages 1 to 6: (a) Displacement field computed by OpenCorr; (b) Displacement field computed by CPD-FEM (coherent point drift finite element method) and (c) Comparison of displacement difference from OpenCorr and CPD-FEM results with error colour bar.

**Table 3**
Statistical error analysis of experimental results.

| Compression stage | Error (mm) | Error (%) | *R* |
|---|---|---|---|
| 1 | $0.0002 \pm 0.0044$ | 0.13 | 0.9976 |
| 2 | $0.0048 \pm 0.0294$ | 2.81 | 0.9797 |
| 3 | $0.0094 \pm 0.0463$ | 3.91 | 0.9780 |
| 4 | $0.0105 \pm 0.0645$ | 3.48 | 0.9780 |
| 5 | $0.0185 \pm 0.0802$ | 4.19 | 0.9782 |
| 6 | $0.0143 \pm 0.0774$ | 3.07 | 0.9873 |

Data are presented as mean $\pm$ standard deviation; *R* is the correlation coefficient.

$$E_s = \sqrt{{E_{xx}}^2 + {E_{yy}}^2 + {E_{zz}}^2} \tag{6}$$

### 2.4. Simulation procedure

Simulations were performed using in-house code in MATLAB (MATLAB 2022b). Firstly, we conducted a self-validation test to assess the flexibility of IA surface motion tracking using the CPD-FEM method. Since our 4D-CTA image data are time-series, we need to select a phase as a reference for motion tracking. Ideally, the final calculated displacements should be the same even if different phases are used as the reference. Therefore, we conducted a self-validation test to assess the flexibility of using this method. Secondly, to further validate the motion-tracking capability of the CPD-FEM method, we conducted a phantom-based experimental analysis with a phantom made of silica gel, which is described in detail in the Appendix. We used the open-source DVC software package: OpenCorr to calculate the displacement fields of the phantom (Jiang, 2023) and compare them with the displacement results from the CPD-FEM method. We then moved to patient-specific models and quantified space displacement, space strain, first principal strain, Von Mises strain, and volume changes during the cardiac cycle for all IAs. Their values were compared between IAs with irregular and normal pulsations using a two-sample *t*-test, and the displacement and strain were normalized (from 0 to 1) before statistical analysis. In this study, a *p* value less than 0.05 was considered statistically significant.

## 3. Results

### 3.1. Self-validation

For the self-validation test, we used the 4D-CTA image data from patient 4 for testing and selected phases 5, 9, 13, and 17 as references for surface motion tracking, respectively. We then calculated the relative displacement of these four sets of results throughout the cardiac cycle, using phase 1 as a reference. The self-validation results are shown in Fig. 2, and we can see that these results are very similar and have the same trend, with the maximum displacements all occurring in phase 10. We also calculated the Euclidean distance (root mean square error) between the aligned point clouds, which is checked for all the patients and shown in Table 2, which is very small compared to the size of the aneurysm and overall displacement.

### 3.2. Experimental validation

Fig. 3 shows the deformation results for the experimental validation according to OpenCorr and CPD-FEM for all compression stages. We can see that the overall displacement field derived by the CPD-FEM is very close to that of the OpenCorr, with a relatively noticeable difference only around the holes in steps 4, 5 and 6, with less than 0.25 *mm*. To further compare the estimation results of CPD-FEM, Table 3 compares the displacement errors, i.e., the averaged spatial difference error and the percentage error, for different compression steps. We can see that the error is very small compared to the displacement, and we also calculated the correlation coefficient ($R > 0.97$) for all compression stage results by Spearman correlation. The results from the above experimental analyses show that the proposed CPD-FEM can accurately estimate the deformation of the phantom model from the measured image data.

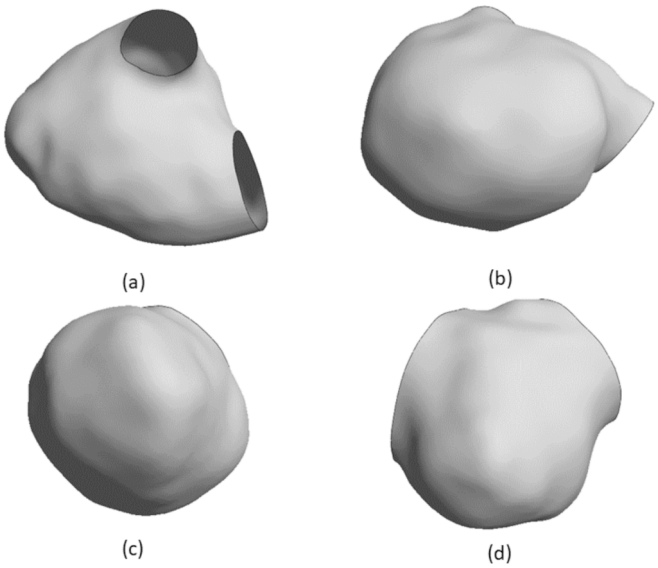


**Fig. 4.** The intracranial aneurysms with irregular pulsation: (a) Patient 1, (b) Patient 2, (c) Patient 3, and (d) Patient 4.

### 3.3. Patient-specific models

Fig. 4 shows the IAs with irregular pulsations of patients 1 to 4. Fig. 5 shows the results of the simulations, including space displacements, space strains, first principal strains and Von Mises strains. The black circle in the first column indicates the location of the irregular pulsation as determined by the clinician through manual assessment with original 3D geometry. It occurred during 15 % to 30 % of the cardiac cycle for patient 1 (Fig. 5(a)), 65 % to 80 % of the cardiac cycle for patient 2 (Fig. 5(b)), 50 % to 65 % of the cardiac cycle for patient 3 (Fig. 5(c)) and 35 % to 50 % of the cardiac cycle for patient 4 (Fig. 5(d)). In the analysis for patient 4, we could only reconstruct 85 % of the cardiac cycle due to image and segmentation quality issues. We observed higher displacement and strain at the locations of irregular pulsations in all four patients. The above analysis shows that the displacement and strain analysis of the aneurysm surface can be used to determine where the irregular pulsation occurs during the cardiac cycle, and a video of the IA deformation and strain throughout the cardiac cycle can be viewed in the supplementary material.

The volume variation during the cardiac cycle was also quantified, as shown in Fig. 6(a). It was found that the total volume change was slightly higher in the aneurysm with irregular pulsations ($5.34 \pm 2.86$ vs $3.71 \pm 1.25$, $p = 0.337$), but it was not statistically significant. Fig. 6(b) to (e) reveals that irregular pulsation of IAs usually occurs during the consecutive ascending or descending phases of the volume change during the cardiac cycle. For the displacement and strain, we used two different ways for comparison. First, we compared the aneurysms' total displacement and strain (averaged value of overall surface points from the minimum volume phase to the maximum volume phase) in the two groups. Second, we compared the stepwise displacement and strain (averaged value overall surface points from the reference phase to all other phases of the cardiac cycle) of the IAs in the two groups. Table 4 shows the total and stepwise displacement and strain comparison between the two groups, and we found that the stepwise first principal strain showed statistically significant differences ($0.20 \pm 0.01$ vs $0.16 \pm 0.02$, $p = 0.033$) between the two groups of aneurysms.

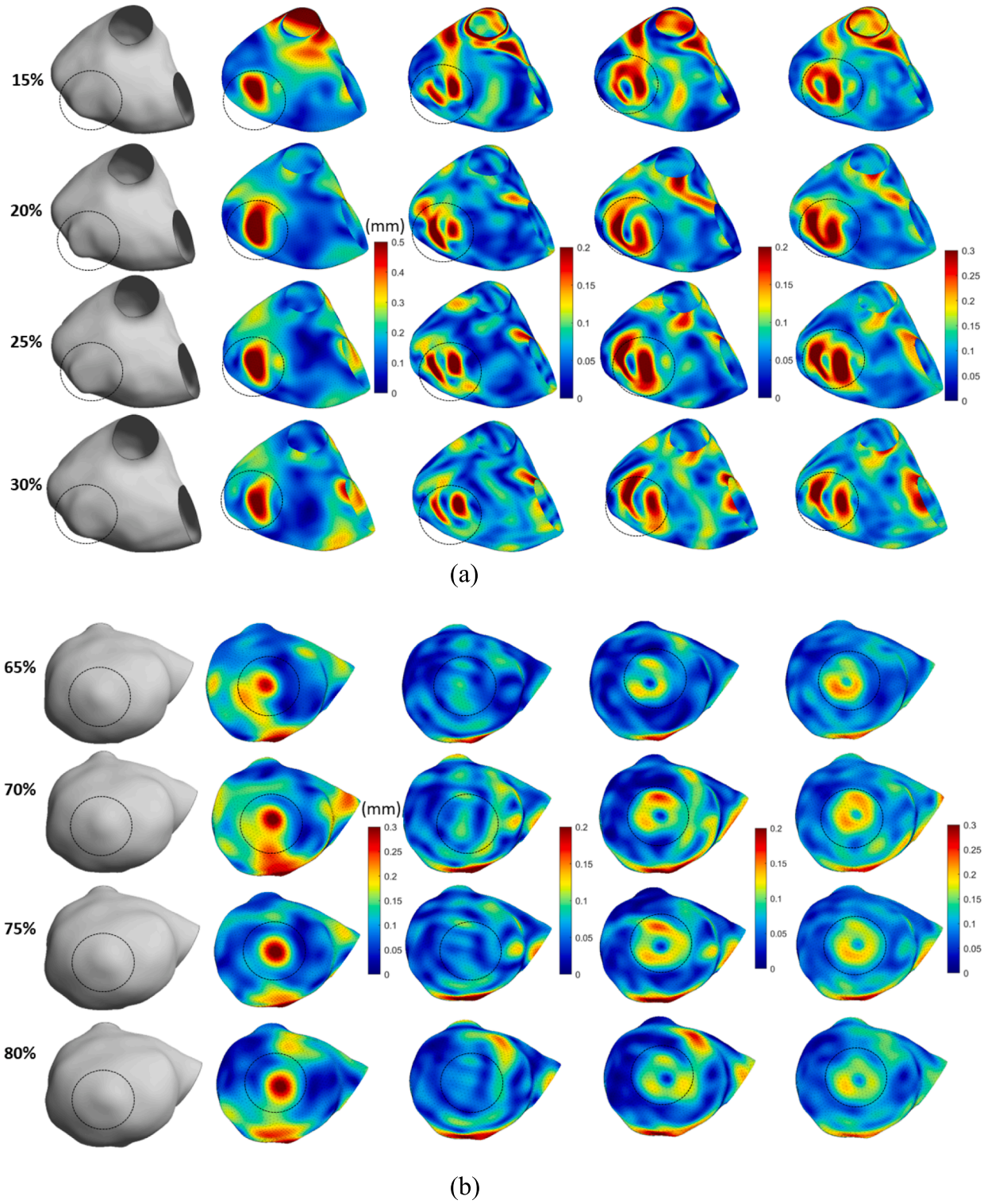


**Fig. 5.** The analysis results of patient-specific intracranial aneurysms with irregular pulsation, the original geometry (1st column) and black circles show the irregular pulsations region; space displacement (2nd column); space strain (3rd column); first principal strain (4th column); and Von Mises strain (5th column): (a) Patient 1; (b) Patient 2; (c) Patient 3 and (d) Patient 4.

## 4. Discussion

### *4.1. Contribution*

The quantification of irregular pulsations based on strain and displacement on the surface of IAs using the CPD-FEM method is a novel concept we propose in this field. In contrast to traditional CFD haemodynamic parameter analysis based on primary static or averaged imaging, the proposed simulation is based on 4D-CTA image data, which can provide dynamic information to visualize abnormal arterial movement. Thus, we can recover the displacement and strain distribution on the surface of the IA during the cardiac cycle. In contrast to existing methods

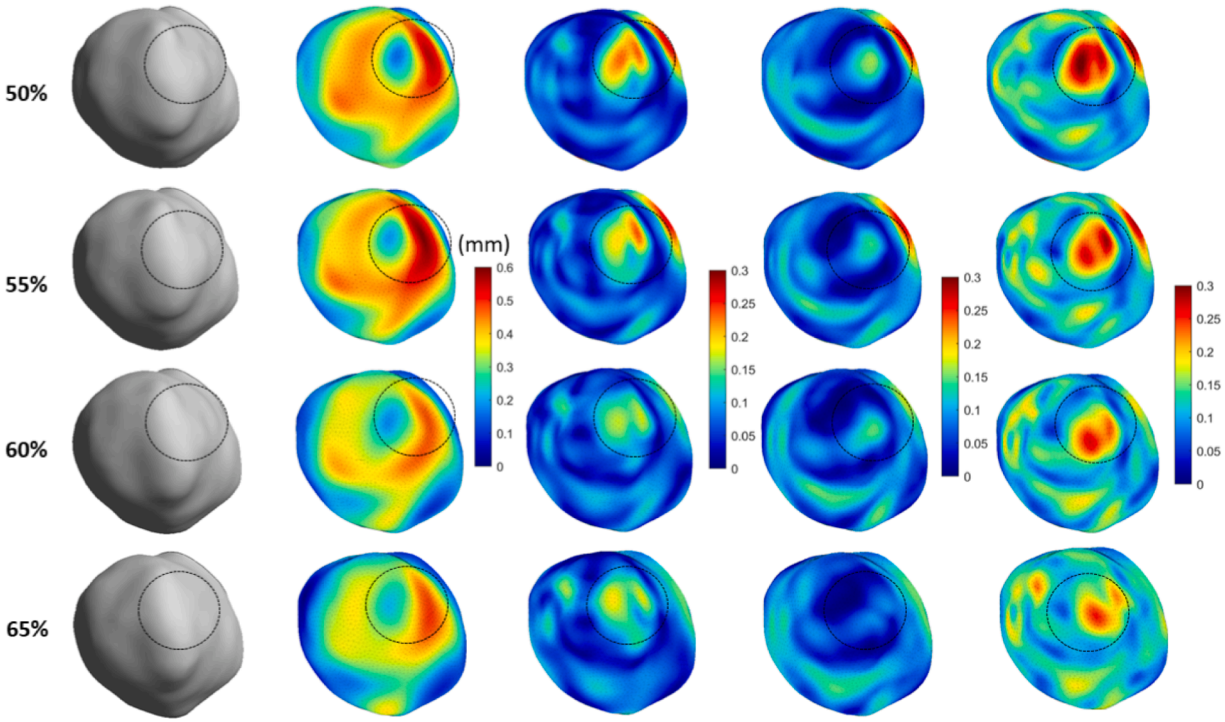


(c)

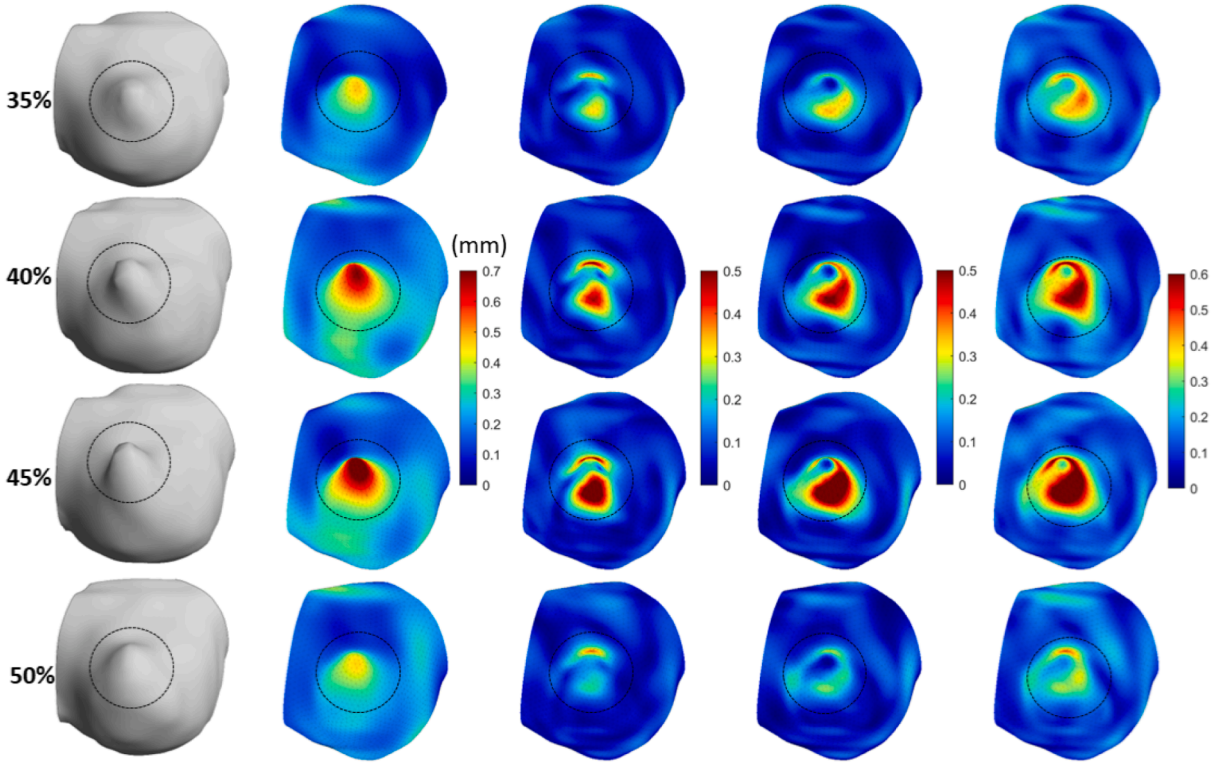


(d)

**Fig. 5.** (*continued*).

for quantifying IA wall motion (Oubel et al., 2010; Pionteck et al., 2024; Stam et al., 2023), the proposed method allows point-to-point comparisons, and the displacement and strain distributions of the entire aneurysm surface can be obtained. Based on the results of the analysis, the strain or displacement is usually higher in locations of irregular pulsations, which can help clinicians better identify irregular pulsations. The experimental analysis results shown in Table 3 demonstrate that the maximum error is less than 5 %, indicating the feasibility and accuracy

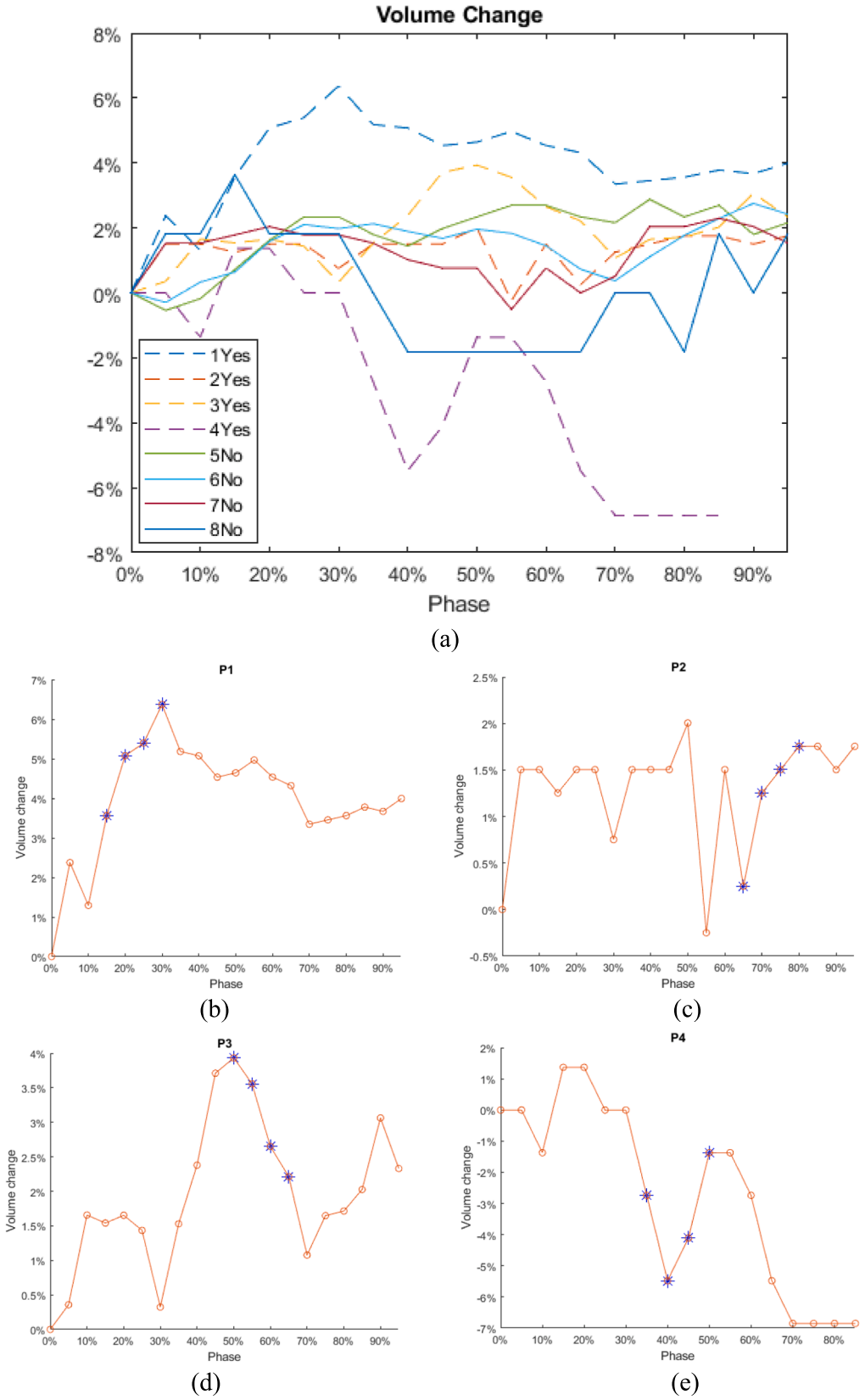


**Fig. 6.** (a) Volume variation during the cardiac cycle; (b) to (e) Volume change during the cardiac cycle of aneurysms with irregular pulsations and blue markers showing the presence of irregular pulsations. (For interpretation of the references to colour in this figure legend, the reader is referred to the web version of this article.)

**Table 4**
Comparison of total and stepwise displacement and strain between the two groups.

| | IAs with irregular pulsation | IAs without irregular pulsation | *P* |
|---|---|---|---|
| **Total space displacement** | 0.39 ± 0.10 | 0.40 ± 0.04 | 0.878 |
| **Total space strain** | 0.26 ± 0.02 | 0.28 ± 0.03 | 0.379 |
| **Total first principal strain** | 0.27 ± 0.04 | 0.26 ± 0.07 | 0.909 |
| **Total Von Mises strain** | 0.29 ± 0.05 | 0.29 ± 0.11 | 0.952 |
| **Stepwise space displacement** | 0.26 ± 0.04 | 0.25 ± 0.05 | 0.841 |
| **Stepwise space strain** | 0.20 ± 0.04 | 0.17 ± 0.02 | 0.372 |
| **Stepwise first principal strain** | 0.20 ± 0.01 | 0.16 ± 0.02 | 0.033 |
| **Stepwise Von Mises strain** | 0.24 ± 0.04 | 0.19 ± 0.02 | 0.087 |

Data are presented as mean ± standard deviation.

of the proposed method.

Additionally, Fig. 5 reveals that irregular pulsations of IAs typically occur at blebs, which are the focally raised locations on the aneurysm. However, this is not always the case. Further analyses involving more patient data or even obtaining multiple cardiac cycle data could better explain this phenomenon. In terms of statistical analysis, it was found that the stepwise first principal strain was significantly higher in aneurysms with irregular than normal pulsations ($0.20 \pm 0.01$ vs $0.16 \pm 0.02$, $p = 0.033$). In contrast, space displacement alone may not be able to quantify the irregular pulsation of the aneurysm, as the rigid body motion of an aneurysm also results in larger displacements. Overall, the deformation parameters of IAs obtained from 4D-CTA-based CPD-FEM dynamic analysis may provide additional information for IA risk assessment.

### 4.2. Limitation

Our study also has several limitations. Firstly, we focused on unruptured IAs size larger than 3 *mm*, thereby excluding smaller aneurysms from consideration. Given the current imaging resolution ($0.31 \times 0.31 \times 0.5$ $mm^3$), we speculate that detecting irregular pulsations in aneurysms smaller than 3 *mm* may prove challenging. Secondly, we assumed the IA as a thin-walled membrane structure for strain calculation, and the reliability of the proposed method can be improved if the actual thickness of the IA can be obtained. Also, the selection of the reference phase is only based on the criterion that the sum of the spatial distances from all surface points of the phase to the centroid is the smallest. Theoretically, aneurysms are pre-deformed in vivo at non-zero pressure, and obtaining a theoretical zero-pressure geometry will help us better quantify displacement, strain, and even stress distributions. Some researchers have proposed a non-invasive method to estimate the zero-pressure configuration of an aneurysm using in vivo imaging reconstructed geometries based on population-averaged material parameters (Raghavan et al., 2006). This approach may be a potential option for defining the reference phase when dealing with large data sets in the future. Moreover, some researchers have proposed a cycle-averaged geometric model to calculate the displacement and strain of abdominal aortic aneurysms (Hegner et al., 2023). However, using an averaged model may lose some essential morphological information when quantifying the irregular pulsation of intracranial aneurysms. Thirdly, the current analysis is only based on data within one cardiac cycle, and comparing results from multiple cardiac cycles could further improve the reliability of the proposed method, e.g. to address volume differences in IAs at the beginning and end of the cardiac cycle. Moreover, our study included only eight patients, and better quantification of irregular pulsations based on strain or displacement distributions may require more data analysis. Finally, although the radiation dose from 4D-CTA is within the safe range, the radiation dose from 4D-CTA acquisition is relatively higher than that from static CTA.

## 5. Conclusions

Irregular pulsations of IAs are thought to be associated with or may indicate a risk of rupture. The proposed work is the very first study to quantify irregular pulsations in IAs using 4D-CTA, and based on the available analyses, the location of the irregular pulsations has higher displacements and strains. Moreover, irregular pulsations usually occur during the consecutive ascending or descending phases of volume changes during the cardiac cycle, and the stepwise first principal strain was statistically significant between aneurysms with irregular pulsations and normal aneurysms. The proposed CPD-FEM method provides a solution for quantifying the irregular pulsations of IAs and may provide additional parameters for the clinical management and assessment of IAs.

In future work, we aim to explore the potential relationship that may exist between irregular pulsation of aneurysms and the risk of rupture by analyzing more patient data. By combining large amounts of patient data and machine learning, we aim to automate risk assessment decisions based on aneurysm surface displacement or strain distribution results. In addition, measurement uncertainty is an essential factor affecting the results of aneurysm displacement estimation, especially when high accuracy and reproducibility are required. Therefore, the quantitative assessment of measurement uncertainty is also one of the future research directions. In addition, with the assurance that the radiation dose is within a safe range, acquiring and analyzing data from multiple cardiac cycles can further increase the reliability of the proposed method.

## CRediT authorship contribution statement

**Hujin Xie:** Writing – review & editing, Writing – original draft, Visualization, Validation, Software, Methodology, Investigation, Conceptualization. **Han Yu:** Writing – review & editing, Methodology, Investigation, Formal analysis. **Hao Wu:** Visualization, Software, Resources, Methodology, Investigation. **Jiaqiu Wang:** Writing – review & editing, Software, Resources, Methodology, Investigation. **Shanglin Wu:** Writing – review & editing, Resources, Data curation. **Jianjian Zhang:** Writing – review & editing, Data curation. **Huilin Zhao:** Writing – review & editing, Supervision, Resources, Data curation, Conceptualization. **Mingyang Yuan:** Investigation, Formal analysis, Data curation. **Jessica Benitez Mendieta:** Investigation, Data curation, Conceptualization. **Haveena Anbananthan:** Software, Resources, Formal analysis. **Craig Winter:** Writing – review & editing, Supervision. **Chengcheng Zhu:** Writing – review & editing, Resources, Investigation, Data curation, Conceptualization. **Zhiyong Li:** Supervision, Funding acquisition, Data curation.

## Declaration of competing interest

The authors declare that they have no known competing financial interests or personal relationships that could have appeared to influence the work reported in this paper.

## Data availability

Data will be made available on request.

## Acknowledgement

The research is partially supported by the National Natural Science Foundation of China (12172089, 12372307, 61821002), ARC

(DP200103492), MRFF (2016165, 2023977), CBT Early Career Researcher Grant (324910-0025/07) and Chengcheng Zhu is supported by United States National Institute of Health (NIH) grants R01HL162743 and R00HL136883.

## Appendix A. Supplementary material

Supplementary data to this article can be found online at https://doi.org/10.1016/j.jbiomech.2024.112269.

## References

Bakker, M.K., Kanning, J.P., Abraham, G., Martinsen, A.E., Winsvold, B.S., Zwart, J.-A., Bourcier, R., Sawada, T., Koido, M., Kamatani, Y., 2023. Genetic risk score for intracranial aneurysms: prediction of subarachnoid hemorrhage and role in clinical heterogeneity. Stroke 54, 810–818.

Can, A., Du, R., 2016. Association of hemodynamic factors with intracranial aneurysm formation and rupture: systematic review and meta-analysis. Neurosurgery 78, 510–520.

Diab, R., Chang, D., Zhu, C., Levitt, M.R., Aksakal, M., Zhao, H.-L., Huynh, T.J., Romero-Sanchez, G., Mossa-Basha, M., 2023. Advanced cross-sectional imaging of cerebral aneurysms. Br. J. Radiol. 96, 20220686.

D'Urso, P.I., Lanzino, G., Cloft, H.J., Kallmes, D.F., 2011. Flow diversion for intracranial aneurysms: a review. Stroke 42, 2363–2368.

Ferrari, F., Cirillo, L., Calbucci, F., Bartiromo, F., Ambrosetto, P., Fioravanti, A., Leonardi, M., 2016. Wall motion at 4D-CT angiography and surgical correlation in unruptured intracranial aneurysms: a pilot study. J. Neurosurg. Sci. 63, 501–508.

Greving, J.P., Wermer, M.J., Brown Jr, R.D., Morita, A., Juvela, S., Yonekura, M., Ishibashi, T., Torner, J.C., Nakayama, T., Rinkel, G.J., 2014. Development of the PHASES score for prediction of risk of rupture of intracranial aneurysms: a pooled analysis of six prospective cohort studies. Lancet Neurol. 13, 59–66.

Gu, Y., Zhang, Y., Luo, M., Zhang, H., Liu, X., Miao, C., 2020. Risk factors for asymptomatic intracranial small aneurysm rupture determined by electrocardiographic-gated 4D computed tomographic (CT) angiography. Med. Sci. Monitor Int. Med. J. Experim. Clin. Res. 26, e921835-921831.

Hayakawa, M., Maeda, S., Sadato, A., Tanaka, T., Kaito, T., Hattori, N., Ganaha, T., Moriya, S., Katada, K., Murayama, K., 2011. Detection of pulsation in ruptured and unruptured cerebral aneurysms by electrocardiographically gated 3-dimensional computed tomographic angiography with a 320-row area detector computed tomography and evaluation of its clinical usefulness. Neurosurgery 69, 843–851.

Hayakawa, M., Tanaka, T., Sadato, A., Adachi, K., Ito, K., Hattori, N., Omi, T., Oheda, M., Katada, K., Murayama, K., 2014. Detection of pulsation in unruptured cerebral aneurysms by ECG-gated 3D-CT angiography (4D-CTA) with 320-row area detector CT (ADCT) and follow-up evaluation results: assessment based on heart rate at the time of scanning. Clin. Neuroradiol. 24, 145–150.

Hegner, A., Wittek, A., Derwich, W., Huß, A., Gámez, A.J., Blase, C., 2023. Using averaged models from 4D ultrasound strain imaging allows to significantly differentiate local wall strains in calcified regions of abdominal aortic aneurysms. Biomech. Model. Mechanobiol. 22, 1709–1727.

Hosseini, S.A., Berg, P., Huang, F., Roloff, C., Janiga, G., Thévenin, D., 2021. Central moments multiple relaxation time LBM for hemodynamic simulations in intracranial aneurysms: An in-vitro validation study using PIV and PC-MRI. Comput. Biol. Med. 131, 104251.

Hu, P., Zhou, H., Yan, T., Miu, H., Xiao, F., Zhu, X., Shu, L., Yang, S., Jin, R., Dou, W., 2023. Deep learning-assisted identification and quantification of aneurysmal subarachnoid hemorrhage in non-contrast CT scans: Development and external validation of Hybrid 2D/3D UNet. Neuroimage 279, 120321.

Humphrey, J., Canham, P., 2000. Structure, mechanical properties, and mechanics of intracranial saccular aneurysms. J. Elasticity Phys. Sci. Solids 61, 49–81.

Jiang, Z., 2023. OpenCorr: An open source library for research and development of digital image correlation. Opt. Lasers Eng. 165, 107566.

Khan, M., Arana, V.T., Najafi, M., MacDonald, D., Natarajan, T., Valen-Sendstad, K., Steinman, D., 2021. On the prevalence of flow instabilities from high-fidelity computational fluid dynamics of intracranial bifurcation aneurysms. J. Biomech. 127, 110683.

Kuroda, J., Kinoshita, M., Tanaka, H., Nishida, T., Nakamura, H., Watanabe, Y., Tomiyama, N., Fujinaka, T., Yoshimine, T., 2012. Cardiac cycle-related volume change in unruptured cerebral aneurysms: a detailed volume quantification study using 4-dimensional CT angiography. Stroke 43, 61–66.

Li, Y., Verrelli, D.I., Yang, W., Qian, Y., Chong, W., 2020. A pilot validation of CFD model results against PIV observations of haemodynamics in intracranial aneurysms treated with flow-diverting stents. J. Biomech. 100, 109590.

Li, Y., Amili, O., Moen, S., Van de Moortele, P.-F., Grande, A., Jagadeesan, B., Coletti, F., 2022. Flow residence time in intracranial aneurysms evaluated by in vitro 4D flow MRI. J. Biomech. 141, 111211.

Lu, J., Zhou, X., Raghavan, M.L., 2008. Inverse method of stress analysis for cerebral aneurysms. Biomech. Model. Mechanobiol. 7, 477–486.

Ma, B., Harbaugh, R.E., Raghavan, M.L., 2004. Three-dimensional geometrical characterization of cerebral aneurysms. Ann. Biomed. Eng. 32, 264–273.

Ma, B., Lu, J., Harbaugh, R.E., Raghavan, M.L., 2007. Nonlinear anisotropic stress analysis of anatomically realistic cerebral aneurysms. J. Biomech. Eng. 129, 88–96.

Myronenko, A., Song, X., 2010. Point set registration: Coherent point drift. IEEE Trans. Pattern Anal. Mach. Intell. 32, 2262–2275.

Oubel, E., Cebral, J., De Craene, M., Blanc, R., Blasco, J., Macho, J., Putman, C., Frangi, A., 2010. Wall motion estimation in intracranial aneurysms. Physiol. Meas. 31, 1119.

Pionteck, A., Abderezaei, J., Fillingham, P., Chuang, Y.-C., Sakai, Y., Belani, P., Rigney, B., De Leacy, R., Fifi, J.T., Chien, A., 2024. Intracranial aneurysm wall displacement depicted by amplified Flow predicts growth. Journal of NeuroInterventional. Surgery.

Raghavan, M., Ma, B., Fillinger, M.F., 2006. Non-invasive determination of zero-pressure geometry of arterial aneurysms. Ann. Biomed. Eng. 34, 1414–1419.

Rinkel, G.J., 2019. Management of patients with unruptured intracranial aneurysms. Curr. Opin. Neurol. 32, 49–53.

Sforza, D.M., Putman, C.M., Cebral, J.R., 2009. Hemodynamics of cerebral aneurysms. Annu. Rev. Fluid Mech. 41, 91–107.

Stam, L.B., Linden, S.M., Oostveen, L.J., Hansen, H.H., Aquarius, R., Slump, C.H., de Korte, C.L., Bartels, R.H., Prokop, M., Boogaarts, H.D., 2023. Dynamic computed tomography angiography for capturing vessel wall motion: a phantom study for optimal image reconstruction. PLoS One 18, e0293353.

Timmins, K.M., van der Schaaf, I.C., Bennink, E., Ruigrok, Y.M., An, X., Baumgartner, M., Bourdon, P., De Feo, R., Di Noto, T., Dubost, F., 2021. Comparing methods of detecting and segmenting unruptured intracranial aneurysms on TOF-MRAS: the ADAM challenge. Neuroimage 238, 118216.

Vanrossomme, A., Eker, O.F., Thiran, J.-P., Courbebaisse, G., Boudjeltia, K.Z., 2015. Intracranial aneurysms: wall motion analysis for prediction of rupture. Am. J. Neuroradiol. 36, 1796–1802.

Vlak, M.H., Algra, A., Brandenburg, R., Rinkel, G.J., 2011. Prevalence of unruptured intracranial aneurysms, with emphasis on sex, age, comorbidity, country, and time period: a systematic review and meta-analysis. Lancet Neurol. 10, 626–636.

Wang, B., Shen, C., Su, Z., Nie, X., Zhao, J., Qiu, S., Li, Y., 2023. Correlation between the rate of morphological changes and rupture of intracranial aneurysms during one cardiac cycle analyzed by 4D-CTA. Front. Neurol. 14.

Xie, H., Wu, H., Wang, J., Mendieta, J.B., Yu, H., Xiang, Y., Anbananthan, H., Zhang, J., Zhao, H., Zhu, Z., 2024. Constrained estimation of intracranial aneurysm surface deformation using 4D-CTA. Comput. Methods Programs Biomed. 244, 107975.

Zhang, J., Li, X., Zhao, B., Zhang, J., Sun, B., Wang, L., Ding, S., Liu, X., Yan, J., Mossa-Basha, M., 2021. Irregular pulsation of intracranial unruptured aneurysm detected by four-dimensional CT angiography is associated with increased estimated rupture risk and conventional risk factors. J. NeuroIntervent. Surg. 13, 854–859.

Zhang, J., Li, X., Zhao, B., Zhang, J., Sun, B., Wang, L., Tian, J., Mossa-Basha, M., Kim, L. J., Yan, J., 2023. Irregular pulsation of aneurysmal wall is associated with symptomatic and ruptured intracranial aneurysms. J. NeuroIntervent. Surg. 15, 91–96.